Design of Wideband Leaky-Wave Antenna Using Sinusoidally Modulated Impedance Surface Based on the Holography Theory

Homayoon Oraizi, *Life Senior Member, IEEE*, Amrollah Amini, Ali Abdolali, *Senior Member, IEEE*, and A. Mehdi Karimimehr

***Abstract*—In this letter, sinusoidally modulated impedance surfaces composed of hexagonal unit cells are used for the implementation of the leaky-wave antennas with frequency scanability in the band of 13–18 GHz. The antenna bandwidth has been studied from two view points—first, from the aspect of the impedance-matching bandwidth and second, from the aspect of the bandwidth scanning of the antenna. In order to improve the performance of the impedance bandwidth, an SIW launcher with a wideband transition is used. In order to improve the frequency-scan capability, a one-dimensional hologram is used. Also the launcher is located at a corner to cancel the destructive effect of the backward radiation. The impedance surface is designed to produce a beam tilt at the angle of 60° at 18 GHz, namely the upper limit of the frequency band. The achieved characteristics of the proposed antenna are 32% bandwidth and angular scan of 22°–60°. A prototype model of the antenna is fabricated and tested as the proof of the concept.**

***Index Terms*—Holographic antennas, impedance surface, leaky-wave antennas, wideband antenna.**

I. Introduction

THE leaky-wave antennas with frequency scanability are suitable for the frequency-modulated continuous wave (FMCW) radar systems. The control of the leaky wave and frequency scanning are produced by the local and partial variation on a waveguide [1]. The main design consideration of the leaky-wave antennas is the objective control of the leaky wave through the waveguide. Various structures have been proposed for these antennas such as the slot waveguide antennas [2].

The application of the holography in antenna engineering was first introduced by Checcaci [3]. Three categories of holograms may be recognized according to the type of excitation: 1) holographic reflectarrays introduced in [4] and [5]; 2) holograms using the leaky-wave mechanism and cylindrical-wave launchers introduced in [6] and [7]; and 3) the one-dimensional (1-D) leaky-wave holograms using the plane-wave launcher first introduced in [8] as a sinusoidally modulated leaky-wave antenna. In the leaky-wave holograms with cylindrical-wave launchers, two simultaneous forward and backward radiation modes are used at the same operating frequency. These two modes have constructive effect at this frequency. Since the scan steps in terms of the frequency for the two forward and backward waves are different, the antenna has a suitable pattern only at a single frequency. In [9], for the prevention of the destructive effects of the forward and backward modes at other frequencies, the cylindrical-wave source is placed at a corner of the hologram. The placement of the cylindrical-wave launchers at the corner is not appropriate because part of the power is lost in the directions where the hologram does not exist. One method of hologram excitation from corners without power loss is the use of planar-wave launchers. In [8], the planar-wave launcher is placed at the front end of the hologram for the excitation of surface waves. A bandwidth of 20% is achieved for the antenna performance. In [10], the same technique is used for the hologram feed system. The antenna bandwidth is achieved by a multilayered hologram in the frequency range 9.5–16 GHz. However, the multilayering of the hologram leads to the complexity of fabrication and increased costs. In [11], capacitively tuned reactance surfaces are applied for the realization of impedance surfaces for the sinusoidally modulated antennas. The achieved operation bandwidth is 22%.

A single-layer leaky-wave hologram antenna with a plane-wave launcher is designed here for 13–18 GHz, which possesses a wide bandwidth and low side lobe levels [10].

Only the hologram forward mode is utilized, and the launcher as the feed system is located at the corner of the hologram, which increases the impedance and radiation bandwidths relative to other reported antennas.

II. Theory of Holography for Antenna Design

The holography theory is used here for the implementation of surface impedances for the pattern synthesis of surface-wave antennas. The holographic theory is based on the principle that a reference-wave (ψ_{ref}) incident on an object produces a scattered wave (ψ_{obj}). Therefore, the interference between the incident and scattered waves will effectively generate the image of the original object. Consequently, if the surface wave as a reference wave (ψ_{ref}) and the desired wave as an object wave (ψ_{obj}) are considered, then the surface impedance required for the antenna-pattern synthesis may be obtained as [6]

$$\eta_{\text{surf}}(x, y) = jX_0\eta_0(1 + M \times \text{Re}\{\psi_{\text{ref}}\psi^*_{\text{obj}}\}) \tag{1}$$

where X_0 is the average amplitude of a normalized surface impedance relative to a free space intrinsic impedance (η_0) and M is the modulation coefficient. For example, for a reference

Manuscript received July 25, 2018; revised August 19, 2018; accepted August 20, 2018. Date of publication August 22, 2018; date of current version October 4, 2018. *(Corresponding author: Homayoon Oraizi.)*

The authors are with the School of Electrical Engineering, Iran University of Science and Technology, Tehran 16844, Iran (e-mail: h_oraizi@iust.ac.ir; amini_am@elec.iust.ac.ir; abdolali@iust.ac.ir; m_karimimehr@elec.iust.ac.ir).

Digital Object Identifier 10.1109/LAWP.2018.2866712

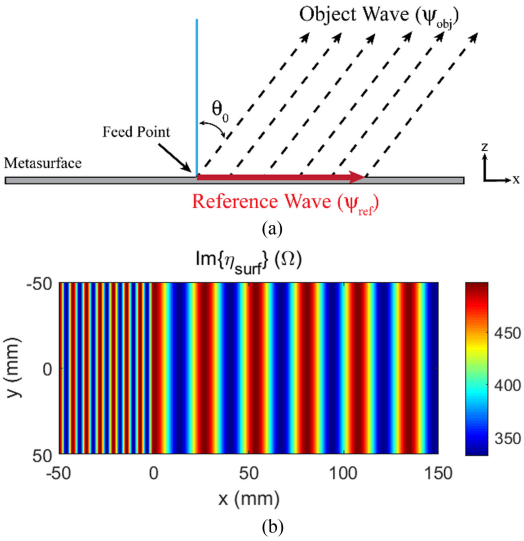

Fig. 1. Interference pattern of the planar-wave source and object wave in the direction $\theta_0 = 60^\circ$ and $\phi_0 = 0^\circ$ at 18 GHz. (a) Direction of the reference and object waves. (b) Impedance pattern.

planar wave and an objective wave as

$$\psi_{\text{ref}} = e^{-jkn|x|} \tag{2}$$

$$\psi_{\text{obj}} = e^{-j(kx\sin\theta_0\cos\phi_0 + ky\sin\theta_0\sin\phi_0)} \tag{3}$$

the surface impedance is

$$\eta_{\text{surf}}(x, y) = jX_0\eta_0(1 + M \times \cos(kx\sin\theta_0\cos\phi_0 + \cdots ky\sin\theta_0\sin\phi_0 - kn|x|)) \tag{4}$$

where θ_0 and ϕ_0 are the main-lobe direction angles [see Fig. 1(a)]. Parameter n is the effective index of the refraction of the surface impedance for the incidence of reference wave considering the periodic nature of surface impedance. The value of n in (2) is equal to the average index of the refraction as [12]

$$n = \sqrt{1 + X_0^2}. \tag{5}$$

Note that (5) is valid when M is small enough. If the reference surface wave is a planar wave traveling in the x-direction, the synthesized surface impedance pattern for the radiation lobe in the direction of $\theta = 60^\circ$ and $\phi_0 = 0^\circ$ at 18 GHz is as shown in Fig. 1(b).

III. Design of Launcher as the Source of Reference Wave

Various launchers have been designed for the sinusoidally modulated surface impedances. For the holographic leaky waves, usually two modes, TE_0 and TM_0, are used as reference waves. The TE_0 mode may be generated by the antipodal Vivaldi antennas [13]. The surface impedances that support the TM_0 mode usually possess a ground plane. Conical monopoles and volcano-smoke antennas are wideband antennas for the excitation of the TM_0 mode. Other antennas for the TM_0 are the SIW horn and the slot quasi-Yagi, which are capable of an integration with microstrip circuits, and also preferable for mmW systems. Since the unit cell is synthesized with the assumption that the TM_0 surface mode is excited, the purity of the surface-wave polarization of the launcher is particularly important. The horn antennas have generally a pure polarization in the end-fire direction. The structure of the proposed launcher is shown in Fig. 2(a). It consists of three parts as follows:

1) Wideband microstrip to the SIW transition, which transforms the Q-TEM mode to the TE_{10} mode. It is based on the configuration proposed in [14].

2) The SIW section.

3) The open aperture for the generation of the surface wave.

All the three parts improve the launcher impedance characteristics. It could be simulated independently by the presence of the antenna.

Therefore, the structure is simulated in the back-to-back configuration. In Table I, the dimensions of the structure after the full-wave optimization are given. The reflection and transmission coefficients of the back-to-back structure are given in Fig. 2(b). Observe that the characteristics of the launcher are acceptable in the range 8.5–18 GHz.

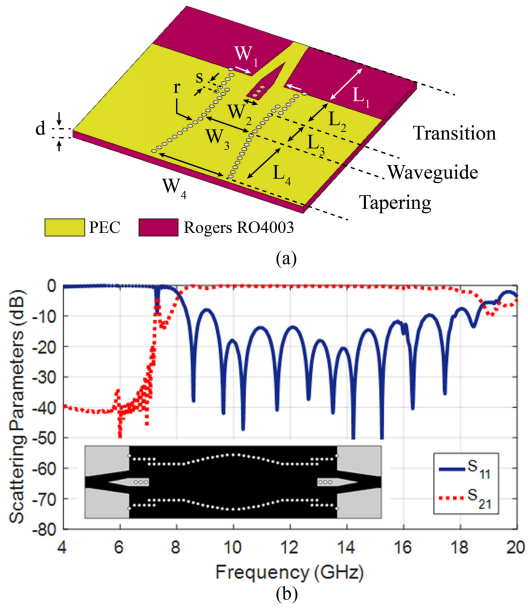

Fig. 2. (a) Geometry of the proposed SIW launcher. (b) Scattering parameters of the proposed back-to-back launcher.

TABLE I
Dimensions of the Launcher in Fig. 2(a)

Parameter	Value (mm)	Parameter	Value (mm)
L_1	13.5	W_3	11
L_2	7.5	W_4	16.6
L_3	9	r	0.5
L_4	15	s	1.5
W_1	7	d	1.524
W_2	2.7		

IV. Proposed Unit Cell

For the configuration of the surface impedance pattern, it is necessary that the dimensions of the unit cell be small, relative to the wavelength. The grounded unit-cell patches (such as square, circular, and hexagonal) are suitable for the implementation of impedance surfaces. In this letter, the hexagonal patches are used for the surface impedance, as shown in Fig. 3. The unit cell with a hexagonal lattice shape is more well behaved considering

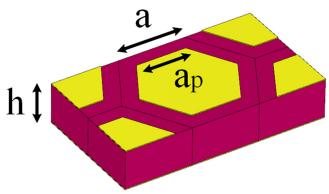

Fig. 3. Geometry of the proposed hexagonal unit cell.

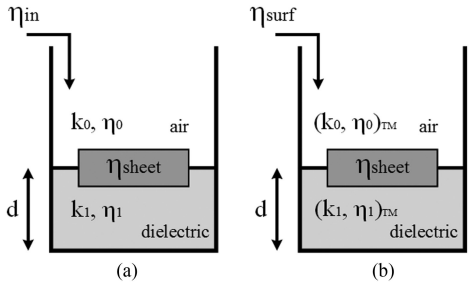

Fig. 4. Equivalent transmission line of the proposed unit cell. (a) Normal-wave incident model. (b) TM-mode wave model.

the dispersion isotropy [15]. For the calculation of its surface impedance, the proposed procedure in [8] is used.

Fig. 4(a) shows the equivalent circuit for the normal wave incidence on an arbitrary-shaped surface impedance with a grounded dielectric substrate. Fig. 4(b) shows the modified equivalent transmission line circuit for the TM-mode surface-wave propagation. The input impedance η_{in} may be obtained by the full-wave simulation, which is related to the reflection coefficient as

$$\eta_{\text{in}} = \eta_0 \frac{1+\Gamma}{1-\Gamma}. \tag{6}$$

The surface impedance for the normal incidence (η_{sheet}) is obtained by the following equation in Fig. 4(a):

$$\frac{1}{\eta_{\text{sheet}}} = \frac{1}{\eta_{\text{in}}} - \frac{1}{j\eta_1 \tan(k_1 d)}. \tag{7}$$

The surface impedance of the incident TM mode (η_{surf}) from the circuit in Fig. 4(b) using η_{sheet} can be obtained as

$$\frac{1}{\eta_{\text{surf}}} = \frac{1}{\eta_{\text{sheet}}} + \frac{1}{j\frac{\eta_0 k_{z1}}{k_0 \epsilon_{r1}} \tan(k_{z1} d)} \tag{8}$$

where

$$k_{z1} = \sqrt{k_0^2(\epsilon_{r1} - 1) + (\frac{\eta_{\text{surf}} k_0}{\eta_0})^2}. \tag{9}$$

The substrate Rogers RO4003 is used with the dielectric constant $\epsilon_r = 3.55$, $\tan\delta = 0.0027$, and $d = 1.524$ mm. The curves of variations of the imaginary parts of η_{in} and η_{surf} at a frequency of 18 GHz as a function of length of the hexagonal edge (a_p) are drawn in Fig. 5. The value of a in Fig. 3 is 2.6 mm.

V. Implementation of the Proposed Leaky-Wave Antenna

According to the foregoing discussion, the configuration of the surface impedance pattern depends on the incident reference

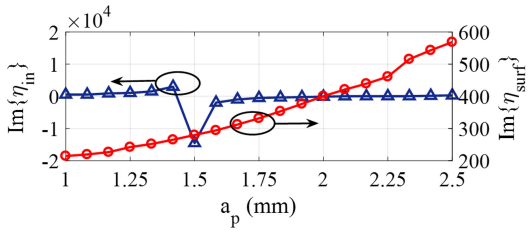

Fig. 5. Curves of variations of the input impedance, and surface impedance of the proposed unit cell at frequency 18 GHz.

wave. The period of surface impedance is obtained by

$$p = \frac{2\pi}{k(\sqrt{1+X_0^2} - \sin\theta_0)}. \tag{10}$$

Equation (10) denotes the relation between direction angle (θ_0) and physical parameters of the antenna ("X_0" and "p"). By choosing the desired angle of radiation for $n = -1$ and fixing either X_0 or p (periodicity), the remaining value may be obtained. The variation of M indicates the depth of modulation and changes the degree of power leakage from a certain length of the structure [8]. The parameter M has no effect on the beam direction of the antenna. Nevertheless, it effects the antenna gain, side-lobe level, and radiation efficiency [8]. On the other hand, the parameters X_0 and M should be selected in such a way that the synthesis of the unit cell does not practically cause any difficulty. For example, the gap produced between two adjacent cells should not be narrower than 0.2 mm, due to the available fabrication technology in the local laboratory.

In this letter, the tilt angle is selected at 60° for 18 GHz. The synthesized surface impedance pattern for the planar-wave incidence is shown in Fig. 1(b). The parameters X_0 and M are selected as 1.1 and 0.2, respectively. Therefore, the period of variation of surface (p) is 26.8 mm as obtained from (10).

The number of unit cells in a period determines the resolution of the synthesis of the surface impedance. Nevertheless, the number of unit cells in a period should be selected in such a way that the computer simulation of the antenna full structure does not prohibitly increase. On the other hand, the number of unit cells should not be too few to worsen the accuracy of the synthesis of the impedance surface. In this case, six unit cells can be accommodated in a period. Therefore, three levels of impedance may be considered according to the curve in Fig. 5. The range of variations of surface impedance for the values of $X_0 = 1.1$ and $M = 0.2$ are $j331.76$, $j414.70$, and $j497.64$. The lengths of sides of hexagons are 1.78, 2.10, and 2.34 mm, respectively.

The geometry of the proposed antenna and the fabricated prototype are shown in Fig. 6.

The measured and simulated results at different frequencies are plotted in Fig. 7. The return loss is less than −10 dB within the frequency band of 13–18 GHz. The beam angles at frequencies 13, 15, and 18 GHz are 22°, 33°, and 60°, respectively. Fig. 8 shows the radiation patterns in a 2-D plane at different frequencies. Its total efficiency and transmission coefficient are shown in Fig. 9.

The transmission coefficient is less than −18 dB in the whole frequency band, which indicates that less power will be reached to port 2. Therefore, the radiation performance of the antenna is good. According to (10), the relationship of the main beam

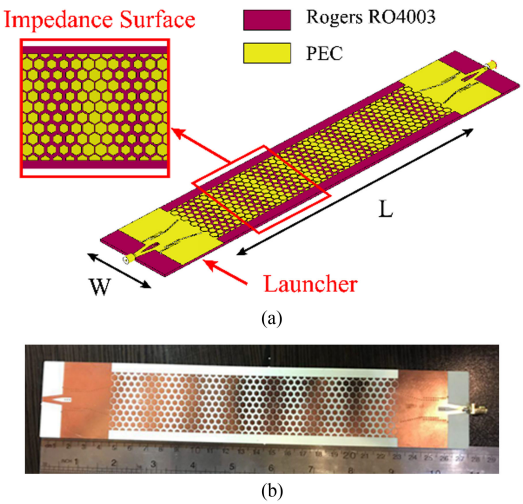

Fig. 6. (a) Geometry of the proposed leaky-wave antenna. (b) Realized prototype of the leaky-wave antenna.

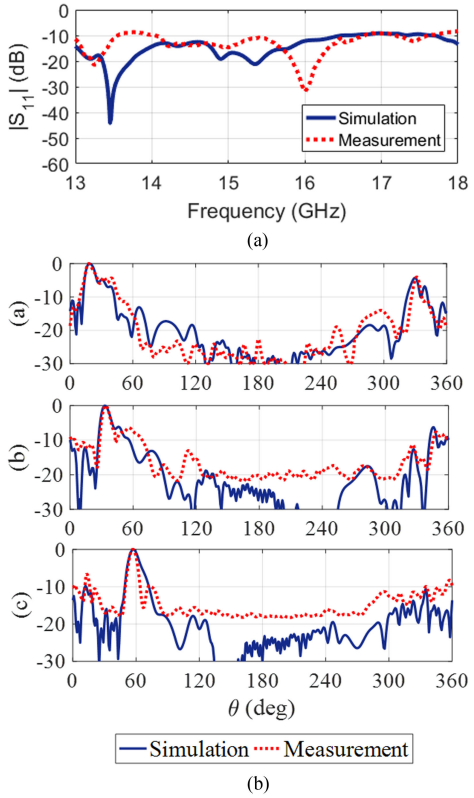

Fig. 7. Simulated and measured results. (a) Reflection coefficient. (b) Normalized pattern in the scan plane for different frequencies.

angle and frequency can be approximately rewritten as

$$\sin\theta_0 = \sqrt{1 + X_0^2} - \frac{2\pi}{kp}. \tag{11}$$

In case of a unilateral leaky-wave antenna (for the dominant leaky mode), the directivity is proportional to β_z and α_x as the following relation:

$$D \propto \frac{\beta_z}{\alpha_x} = \frac{\sqrt{\omega^2\mu_0\epsilon_0 - (\kappa - \frac{2\pi}{d})^2}}{\alpha_x} \tag{12}$$

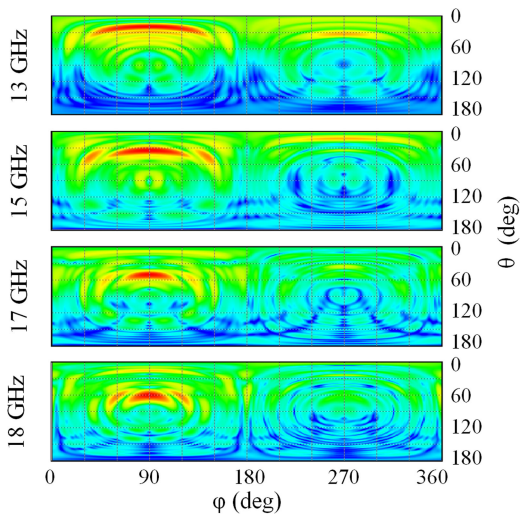

Fig. 8. Simulated radiation patterns of the leaky-wave antenna at frequencies 13, 15, 17, and 18 GHz.

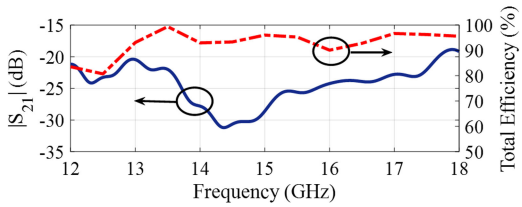

Fig. 9. Simulated transmission coefficient and total efficiency of the antenna.

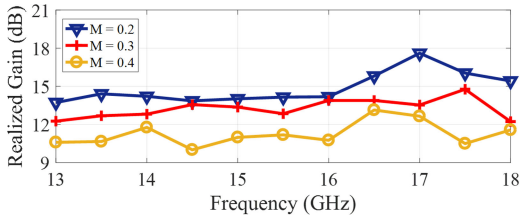

Fig. 10. Maximum realized gain of the antenna for different modulation depths.

where κ is the fundamental harmonic of the wavenumber in the x-direction. Therefore, at lower frequencies, the gain gets lower and the main beam angle decreases. Also, larger values of M lead to larger values of α_x, and therefore, from (12) the gain becomes smaller. Fig. 10 shows the variation of the maximum realized gain for different values of the modulation depth. With an increasing modulation depth, the realized gain decreases.

VI. Conclusion

The theory of holography and sinusoidally modulated impedance surfaces are used to design a leaky-wave antenna in the 13–18 GHz frequency band. The unit cells are composed of hexagonal unit cells, which are suitable for any polarization of incident waves. The SIW horn launcher with an end-fire radiation is used for the excitation of the TM_0 mode. It performs well in the whole desired band and is suitable for the FMCW radar systems.

REFERENCES

[1] J. H. Choi and T. Itoh, "Beam-scanning leaky-wave antennas," in *Handbook of Antenna Technologies*, Z. Chen, D. Liu, H. Nakano, X. Qing, and T. Zwick, Eds., Singapore: Springer-Verlag, 2016, pp. 1–33.

[2] F. L. Whetten and C. A. Balanis, "Meandering long slot leaky-wave waveguide-antennas," *IEEE Trans. Antennas Propag.*, vol. 39, no. 11, pp. 1553–1560, Nov. 1991.

[3] P. Checcacci, V. Russo, and A. Scheggi, "Holographic antennas," *IEEE Trans. Antennas Propag.*, vol. 18, no. 6, pp. 811–813, Nov. 1970.

[4] D. Liu *et al.*, "A horn-fed frequency scanning holographic antenna based on generalized law of reflection," *Sci. Rep.*, vol. 6, 2016, Art. no. 31338, doi: 10.1038/srep31338.

[5] M. Karimipour and N. Komjani, "Holographic-inspired multibeam reflectarray with linear polarization," *IEEE Trans. Antennas Propag.*, vol. 66, no. 6, pp. 2870–2882, Jun. 2018.

[6] B. H. Fong, J. S. Colburn, J. J. Ottusch, J. L. Visher, and D. F. Sievenpiper, "Scalar and tensor holographic artificial impedance surfaces," *IEEE Trans. Antennas Propag.*, vol. 58, no. 10, pp. 3212–3221, Oct. 2010.

[7] G. Minatti, F. Caminita, E. Martini, M. Sabbadini, and S. Maci, "Synthesis of modulated-metasurface antennas with amplitude, phase, and polarization control," *IEEE Trans. Antennas Propag.*, vol. 64, no. 9, pp. 3907–3919, Sep. 2016.

[8] A. M. Patel and A. Grbic, "A printed leaky-wave antenna based on a sinusoidally-modulated reactance surface," *IEEE Trans. Antennas Propag.*, vol. 59, no. 6, pp. 2087–2096, Jun. 2011.

[9] Y. B. Li, X. Wan, B. G. Cai, Q. Cheng, and T. J. Cui, "Frequency-controls of electromagnetic multi-beam scanning by metasurfaces," *Sci. Rep.*, vol. 4, 2014, Art. no. 6921.

[10] S. Pandi, C. A. Balanis, and C. R. Birtcher, "Analysis of wideband multilayered sinusoidally modulated metasurface," *IEEE Antennas Wireless Propag. Lett.*, vol. 15, pp. 1491–1494, 2016.

[11] A. H. Panaretos and D. H. Werner, "Leaky-wave antennas based on capacitively tuned modulated reactance surfaces," *IEEE Antennas Wireless Propag. Lett.*, vol. 15, pp. 678–681, 2016.

[12] Y. B. Li *et al.*, "Holographic leaky-wave metasurfaces for dual-sensor imaging," *Sci. Rep.*, vol. 5, 2015, Art. no. 18170, doi: 10.1038/srep18170.

[13] C. Rusch, J. Schfer, H. Gulan, P. Pahl, and T. Zwick, "Holographic mmW-antennas with TE_0 and TM_0 surface wave launchers for frequency-scanning FMCW-radars," *IEEE Trans. Antennas Propag.*, vol. 63, no. 4, pp. 1603–1613, Apr. 2015.

[14] D. K. Cho and H. Y. Lee, "A new broadband microstrip-to-SIW transition using parallel HMSIW," *J. Electromagn. Eng. Sci.*, vol. 12, no. 2, pp. 171–175, 2012.

[15] M. Li, S. Q. Xiao, and D. F. Sievenpiper, "Polarization-insensitive holographic surfaces with broadside radiation," *IEEE Trans. Antennas Propag.*, vol. 64, no. 12, pp. 5272–5280, Dec. 2016.